Chapter 13

Validation of a Hemi-Variational Block-Based Approach to the Modelling of Common In-plane Failures in Masonry Structures

José Manuel Torres Espino, Jaime Heman Espinoza Sandoval, Chuong Anthony Tran, Roberto Fedele, Emilio Turco, Francesco dell'Isola, Luca Placidi, Anil Misra, Francisco James León Trujillo, and Emilio Barchiesi

José Manuel Torres Espino · Jaime Heman Espinoza Sandoval · Francisco James León Trujillo
Universidad de Lima, Instituto de Investigación Científica, Santiago de Surco, Peru,
e-mail: 20181896@aloe.ulima.edu.pe, jhespino@ulima.edu.pe, fleon@ulima.edu.pe

Chuong Anthony Tran · Francesco dell'Isola
Università degli Studi dell'Aquila, Dipartimento di Ingegneria Civile, Edile-Architettura, Ambientale (DICEAA) & Università degli Studi dell'Aquila, International Research Center for the Mathematics and Mechanics of Complex Systems (M&MoCS), L'Aquila, Italy,
e-mail: tcanth@outlook.com, francesco.dellisola@univaq.it

Roberto Fedele
Politecnico di Milano, Dipartimento di Ingegneria Civile e Ambientale (DICA), Milan & Università degli Studi dell'Aquila, International Research Center for the Mathematics and Mechanics of Complex Systems (M&MoCS), L'Aquila, Italy,
e-mail: roberto.fedele@polimi.it

Emilio Turco
Università degli Studi di Sassari, Dipartimento di Architettura, design e urbanistica (DADU), Alghero & Università degli Studi dell'Aquila, International Research Center for the Mathematics and Mechanics of Complex Systems (M&MoCS), L'Aquila, Italy,
e-mail: eturco@uniss.it

Luca Placidi
Uninettuno International Telematic University, Faculty of Engineering, Rome & Università degli Studi dell'Aquila, International Research Center for the Mathematics and Mechanics of Complex Systems (M&MoCS), L'Aquila, Italy,
e-mail: luca.placidi@uninettunouniversity.net

Anil Misra
Civil, Environmental and Architectural Engineering Department, University of Kansas, Lawrence, USA & Università degli Studi dell'Aquila, International Research Center for the Mathematics and Mechanics of Complex Systems (M&MoCS), L'Aquila, Italy,
e-mail: amisra@ku.edu

Emilio Barchiesi
Università degli Studi di Sassari, Dipartimento di Architettura, design e urbanistica (DADU), Alghero, Università degli Studi dell'Aquila, International Research Center for the Mathematics and Mechanics of Complex Systems (M&MoCS), L'Aquila, Italy & Universidad de Lima, Instituto de Investigación Científica, Santiago de Surco, Peru,
e-mail: ebarchiesi@uniss.it

Abstract Numerical simulations of several planar failure modes of masonry structures are presented, based on the model and solving code from a recent hemivariational block-based model inspired from granular micromechanics (Tran et al. [33]). The numerical tests include a comparison with literature results for a constant shearing load, a parametric study of the influence of mortar thickness, and the simulation of common failures such as bending, shear sliding, and rocking. The results show that the studied model is able to capture common failure modes. Conclusions and insights towards the extension of the studied model are then given.

Key words: Masonry structures · Block-Based model · Masonry failure · Variational model · Hemivariational model · numerical simulations

13.1 Introduction

Masonry or infill walls, formed by brick units joined together by mortar, has been used since ancient times and is still common today, including in reinforced concrete buildings. Generally, masonry elements are used to close or delimit certain spaces, although in some cases they help to support the loads to which a structure is attached, fulfilling the function of a bearing wall. When analyzing structures and evaluating their performance in response to a seismic event, it is very common not to take into account the fill walls, since they are frequently categorized as non-structural elements, assuming that they do not contribute to the rigidity of the structure, and therefore become considered as secondary elements. However, post-quake assessments show that the failure or detachment of the infill walls are responsible for large losses of human life or require large investments for repair [1].

Therefore, it is necessary to provide a more in-depth investigation into the behavior of masonry, which is a very complex issue to address, given that its behavior involves a number of factors that present a great variability, such as: the properties of mortar, the properties of bricks or masonry elements, the quality of labor, the thickness of the mortar layer, the type of bricks, etc. [2].

There were several attempts to incorporate infill walls in the analysis of a structure, such as the contribution of [3], which is still used in certain analyses. According to this proposal, the masonry enclosed between two adjacent columns could be replaced by connecting rod-type elements working under axial load. This approach can be considered as a macro-modeling of masonry walls.

However, thanks to computational advances, it is feasible to resort to micro-modeling, where it is possible to replace the bricks with homogeneous units joined by a layer of mortar with homogeneous properties. In this way, the origin of the faults and the monitoring of these faults in a wall could be detected in a much more precise way, using numerical methods such as finite elements [4, 5] or other ones. More specifically, mixed finite element methods have also been used for the elastoplastic [6] and multiscale [7] analysis of historical masonry structures.

There are several forms of micro-modeling that have been developed, as well as various approaches to model the way masonry units interact with mortar. One such modeling approach lies in using variational principles. Those principles have had a fundamental historical role in deriving mechanical models; we refer the interested reader to [8]-[10] for general historical information about those approaches, [11] for a synthetic presentation and interpretation, and [12, 13] for specific insights regarding the development generalized theories derived from variational principles. One of the advantages of such principles is their self-consistency: they lead to mathematically well-posed problems, as presented in [14, 15]. Variational principles can be declined into different specific versions, depending on how refined one wants their model to be. The simplest example would be the principle of minimum potential energy [16]. It can be generalized into other minimization principles, such as least action principle [17]-[19]. As presented by [20], least action principles can themselves be generalized into virtual work or power principles [21]-[23] or, in the case of variational inequalities, maximum-energy release principles [14, 24].

One way to take advantage of the modeling capabilities of variational principles while accounting for a precise geometrical description of the studied system is to base such principles on discrete kinematics. Indeed, the resulting models allow a refined description of the specific characteristics of the system to be modeled [25]-[28]. This makes them most useful when complex behaviours are arising from complex structures [29]-[32]. The specific example of discrete description which is used in the present work is the "block-based" approach to masonry modeling.

The present work gathers precisely the contributions of Tran et al. [33], who propose the micro-modeling of masonry with a discrete approach, where the base element is an "augmented brick" made of a brick (which is assumed rigid) and a layer of surrounding mortar. Such augmented masonry units kinematically have the possibility of planar translations and rotations in response to an external action that can act on the wall. In this approach, given the rigidity of masonry units, it can be considered that there are certain energy barriers that impose fault behaviors only in the mortar.

In fact, many recent studies on the numerical modeling of masonry have been based on the consideration of rigid blocks that interact with each other through their contact surfaces [34]-[36]. These surfaces, when interacting, tend to compress the mortar at the same time that a cutting effect is generated that tries to cause the sliding of one unit over another, so the role of friction is vital. The development of these approaches is based on variational calculation and Heyman's limit analysis.

The interest of this work has focused on expanding the proposal of Tran et al. [33], which is a numerical modeling of masonry walls based on micro-modeling. Indeed, the model proposed in their work was adapted from continuous granular micromechanics models. Such models have been studied in many recent research efforts [37]-[41], in order to model precisely the grain interactions and their effect on the global behavior [42]-[44]. More specifically, the model studied by Tran et al. is inspired from a recent hemivariational approach to granular micromechanics [24]-[45].

In the present work, we will study how such a model is able to predict several types of faults which have been reported as common in the evaluation of walls. In this way, different masonry walls will be subjected to a progressive monotonous load, evidencing different types of failures, as well as validate the model with other studies.
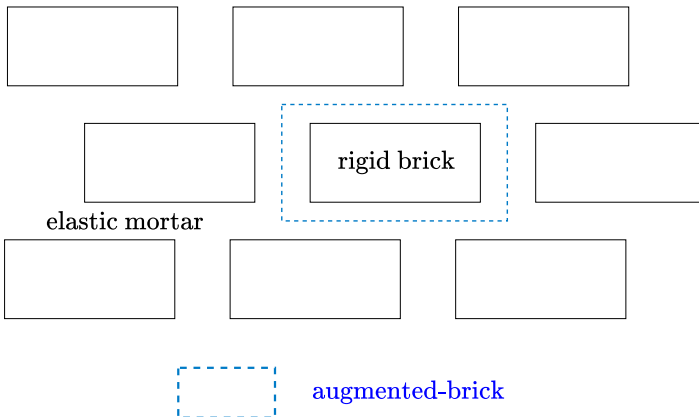
13.2 Mathematical Formulation

The present mathematical formulation is based on the model reported in [33], where more details can be seen for this approach. First, a masonry structure is considered as being formed by rigid bricks with a layer of mortar around. As seen in Fig. 13.1, each of these mortar brick blocks that make up the structure will be regular and identical, and will be called augmented bricks. Since the (internal) bricks are rigid, only the mortar will suffer deformations and damage.

13.2.1 Vertex Springs and Stiffnesses

The elastic behavior of the mortar will be modeled using two springs at the extremities of the contact surface between every pair of neighboring augmented bricks. The elongation of the spring, applying elementary operations of linear algebra, can be calculated as:

$$\underline{\Delta r_v} = \left[\underline{R}_{\theta'} - \underline{I}\right] \cdot \underline{C'S'} - \left[\underline{R}_{\theta} - \underline{I}\right] \cdot \underline{CS} + u_\eta \underline{\eta} + u_\tau \underline{\tau} \tag{13.1}$$

elastic mortar

rigid brick

augmented-brick

Fig. 13.1: An augmented-brick is defined as a rigid brick together with its surrounding layer of elastic mortar [33].

Where Δr_ν represents the elongation of a vertex spring ν, and $\underline{R}_\theta$, $\underline{R}_{\theta'}$ are rotation matrices. The rest of the parameters correspond to geometric values that can be observed in Figure 13.2. This equation indicates that if we know the relative rotations and the relative displacements between a pair of augmented bricks, we can know the elongation of the two vertex springs that join them.

The stiffnesses $k_{\nu,d}^{\eta,t}$, $k_{\nu,d}^{\eta,c}$ and $k_{\nu,d}^{\tau}$ are now defined. The indices η, t, c, ν, τ, d mean: normal, tension, compression, vertex spring, tangential and damage respectively. In addition, damages $D_\nu^{\eta,t}$, $D_\nu^{\eta,c}$ and D_ν^{τ} are introduced as belonging to $[0,1]$. They are the normal (tension and compression) and tangential damages, respectively, associated with each stiffness. f_S is a surface factor that takes into account the contact surface area between the augmented bricks. It can be expressed as half the ratio of

(a) Vertex springs for horizontal neighbours.

(b) Vertex springs for vertical neighbours.
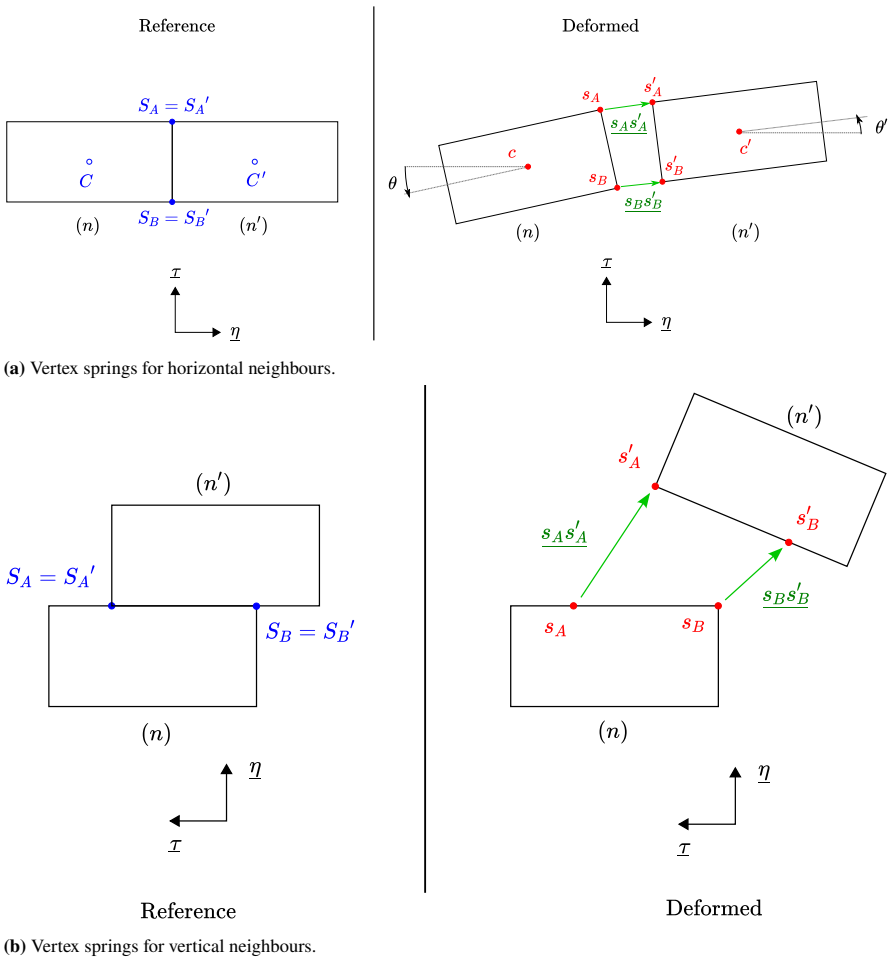
Fig. 13.2: Vertex springs for a pair of augmented-bricks (n, n') [33].

the length of the shared segment and the total length of the associated brick.

$$k_{\nu,d}^{\eta,t} = f_S \, k_\nu^{\eta,t} \left(1 - D_\nu^{\eta,t}\right), \quad \text{(normal, tension)}$$
$$k_{\nu,d}^{\eta,c} = f_S \, k_\nu^{\eta,c} \left(1 - D_\nu^{\eta,c}\right), \quad \text{(normal, compression)} \qquad (13.2)$$
$$k_{\nu,d}^{\tau} = f_S \, k_\nu^{\tau} \left(1 - D_\nu^{\tau}\right), \qquad \text{(tangential)}$$

13.2.2 Deformation Energy and Impenetrability Potential

Because the internal bricks are rigid, an energy barrier will be used to prevent them from overlapping. For this purpose, the elastic deformation energy associated with the relative displacement of a vertex spring is defined as:

$$^{(n,n')}\mathcal{U}^\nu = \frac{C_\nu}{\underline{\Delta r_\nu} \cdot \underline{\eta} - \sigma} + \frac{1}{2} k_{\nu,d}^\tau \left(\underline{\Delta r_\nu} \cdot \underline{\tau}\right)^2 \qquad (13.3)$$

The compression component of this potential energy referred to a fixed pair of augmented bricks (n, n') can have two forms. It shall be quadratic until the normal relative displacement $\underline{\Delta r_\nu} \cdot \underline{\eta}$ reaches a limit u_η^* (defined as negative by being in compression). Beyond that limit, the normal potential energy becomes an inverse function, which has its asymptote equal to σ, whose absolute value is equal to half the thickness of the mortar. So, as normal relative displacement tends to σ, potential energy tends to infinity. In this way, the normal potential energy, depending on its relative displacement, becomes:

$$\begin{cases} \mathcal{U}_{\eta,\text{wall}}^\nu = \dfrac{C_\nu}{\left(\underline{\Delta r_\nu} \cdot \underline{\eta} - \sigma\right)} + \mathcal{E}_0 & \text{if } s < \underline{\Delta r_\nu} \cdot \underline{\eta} < u_\eta^* \\[4mm] \mathcal{U}_{\eta,\text{quad}}^\nu = \dfrac{1}{2} k_{\nu,d}^\eta \left(\underline{\Delta r_\nu} \cdot \underline{\eta}\right)^2 & \text{if } u_\eta^* < \underline{\Delta r_\nu} \cdot \underline{\eta} \end{cases} \qquad (13.4)$$

C_ν and $\mathcal{E}_0$ are parameters that adjust the potential for impenetrability. It can be shown that, when the values of these new parameters are:

$$u_\eta^* = \frac{\sigma}{3}, \quad C_\nu = \frac{4}{27} k_{\nu,d}^\eta \, |\sigma|^3, \quad \mathcal{E}_0 = -\frac{1}{6} k_\nu^\eta \sigma^2,$$

the resulting function becomes twice continuously differentiable. This will allow the calculation of local rigidities detailed in later sections.

13.2.3 Damage Laws

The dissipated energy can be defined for each vertex spring as a function of the damage introduced in the stiffness of the Eq. (13.2). These functions are described by Timofeev et al. [45] where the formulation can be seen in more detail. The main idea of this dissipated energy is that it takes into account the anisotropic behavior that exists in granular materials, where it is known that there is a greater resistance in compression than in tension and/or shear (tangential). As described in [45], when applying the considered hemivariational principle, the dissipated energy leads to the following damage thresholds, in the normal (tension and compression) and tangential directions:

$$
\begin{cases}
D_v^{\eta,t} = 1 - \exp\left(-\dfrac{\underline{\Delta r_v} \cdot \underline{\eta}}{B_v^{\eta,t}} \right) \\[3mm]
D_v^{\eta,c} = \dfrac{2}{\pi} \arctan\left(-\dfrac{\underline{\Delta r_v} \cdot \underline{\eta}}{B_v^{\eta,c}} \right) \\[3mm]
D_v^{\tau} = 1 - \exp\left(-\dfrac{\left|\underline{\Delta r_v} \cdot \underline{\tau}\right|}{B_v^{\tau}} \right)
\end{cases}
\tag{13.5}
$$

where:

$$
B_v^{\tau} =
\begin{cases}
B_{v0}^{\tau}, & \text{if } \underline{\Delta r_v} \cdot \underline{\eta} > 0 \\[2mm]
B_{v0}^{\tau} - \alpha_2 \, \underline{\Delta r_v} \cdot \underline{\eta}, & \text{if } \dfrac{1-\alpha_1}{\alpha_2} B_{v0}^{\tau} \leq \underline{\Delta r_v} \cdot \underline{\eta} \leq 0 \\[2mm]
\alpha_1 \, B_{v0}^{\tau}, & \text{if } \underline{\Delta r_v} \cdot \underline{\eta} < \dfrac{1-\alpha_1}{\alpha_2} B_{v0}^{\tau}
\end{cases}
\tag{13.6}
$$

The displayed values of B_v^{τ} allow damage to continue to increase or to be maintained. The values of B_{v0}^{τ}, α_1 and α_2 model the asymmetry between tension and compression. It is also important to understand the behavior of these functions in the evolution of damage. It can be observed graphically that the tension damage function $D_v^{\eta,t}$ converges to 1 faster than the compression damage function $D_v^{\eta,c}$, when the spring elongation takes large values (positive in tension, negative in compression).

13.2.4 Principle of Minimum Potential Energy

Although the base model presented by Timofeev et al. [45] considered a hemivariational principle, in the present work we will follow the same presentation as Tran et al. [33], who take the damage equations as damage laws independently from the elastic equations. Thus, for a fixed damage state of the masonry system, the elastic equations can be derived from a usual principle of minimum potential energy. Such a separation is legitimate since it is used in the solving algorithm on which is based the program used for the numerical simulations presented in the Results section.

The total potential energy is thus defined as the sum of all deformation energies for every augmented brick pairs (n, n') having v_A and v_B as pairs of vertex springs.

$$\mathcal{E} = \sum_{(n,n')} \left({}^{(n,n')}\mathcal{U}^{v_A} + {}^{(n,n')}\mathcal{U}^{v_B} \right) \tag{13.7}$$

Thus, the stationarity condition for the total potential energy shall be given by equalizing the gradient of the total energy to the null vector: $\nabla \mathcal{E} = \underline{0}$.

13.2.5 Numerical Model

For the numerical model used by Tran et al. [33] a system of $N = n_x \times n_y$ bricks arranged in a regular pattern is considered, as seen in Figure 13.3. Each augmented brick is l_x wide and l_y high. The mortar layer between two bricks is l_m thick. A ratio $\alpha \in (0, 1)$ is defined to represent the horizontal space or overlap between two adjacent rows.

The numerical variables for the calculation of iteration i are: U^i the list of all kinematic variables (displacements and rotations), D^i the list of all damages, K^i the stiffness matrix and b^i the loads. Those loads will be calculated from imposed displacements, instead of external forces.
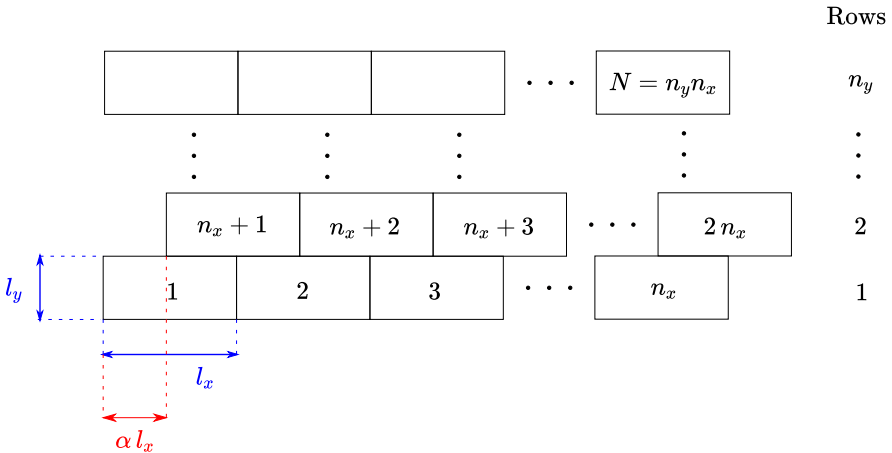

Fig. 13.3: Numerical masonry model considered in this work [33].

13.2.6 Stiffness Matrix

The local stiffnesses for a fixed pair of augmented bricks (n, n') and a fixed pair of vertex springs v are calculated from the second order gradient of the deformation energy $^{(n,n')}\mathcal{U}^v$. Then, each of these local stiffnesses are assembled into a global stiffness matrix.

$$^{(n,n')}K_v(u_\eta, u_\tau, \theta, \theta') := \nabla^2 \left[^{(n,n')}\mathcal{U}^v(u_\eta, u_\tau, \theta, \theta') \right] \tag{13.8}$$

13.2.7 Algorithm

The algorithm for performing numerical calculations is now described. For an iteration n that has already been calculated, the global displacements and rotations U^n, the damages D^n, the stiffness matrix K^n and the load matrix b^n, are known.

For the next step $(n+1)$, the displacements U^{n+1} are unknown, so the increment of the displacement δU^{n+1} will be calculated. It is defined such that:

$$U^{(n+1)} = U^{(n)} + \delta U^{(n+1)} \tag{13.9}$$

In addition, the loads shall be held as follows:

$$b^{(n+1)} = b^{(n)} + \delta b^{(n+1)} \tag{13.10}$$

By elementary matrix operations and by relating the stiffness matrix to displacements and loads, the displacement increase is obtained:

$$\delta U^{(n+1)} = \left(\left[K^{(n)} \right]^{-1} - \left[K^{(n-1)} \right]^{-1} \right) \cdot b^{(n)} + \left[K^{(n)} \right]^{-1} \cdot \delta b^{(n+1)} \tag{13.11}$$

In this way, with equation (11) we can calculate the increment of the displacement δU^{n+1} and with it, perform the calculation of the displacement U^{n+1}, which then allows to update the damage D^{n+1} and the stiffness matrix K^{n+1}.

13.3 Results

In this section, four case studies will be described with the aim of expanding the descriptive results that can be obtained with the model described by Tran et al. [33]. The first corresponds to a comparative result of a simple wall. The second assesses the influence of mortar on masonry behavior, while the last two aim to visualize and explain some common in-plane failure phenomena.

13.3.1 Comparative Result

In order to numerically compare the model formulated by Tran et al. [33], it is intended to evaluate a simple masonry wall subjected to a lateral monotone force on its superior side. Preciado [46] evaluated this scenario by the finite element method in order to validate its proposed model. The study model can be seen graphically in Fig. 13.4.

The geometric parameters of this model are detailed below. The width l_x and height l_y correspond to 0.31 meters and 0.20 meters, respectively. In addition, the mortar thickness l_m is equal to 0.01 meters. It should be taken into account that both the width and height correspond to dimensions of the augmented bricks. The elastic rigidities and damage parameters used in the model can be seen in Table 13.1. In this way, the results were obtained in a Force-Displacement graph of the top of the masonry wall. The result shows a similar behavior with the one evaluated in [46],
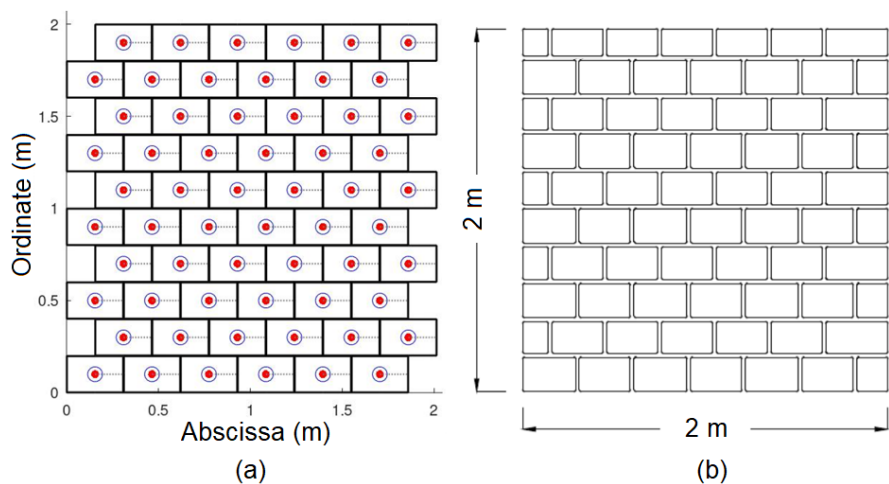
Fig. 13.4: Masonry: (a) Masonry model of the present work. (b) Masonry wall studied in [46].

Table 13.1: Elastic stiffnesses and damage parameters..

Parameter	Value	Unit
$k_\nu^{\eta,t}$	2.05×10^8	N/m
$k_\nu^{\eta,c}$	2.05×10^8	N/m
k_ν^{τ}	2.271×10^8	N/m
$B_\nu^{\eta,t}$	6×10^{-5}	m
$B_\nu^{\eta,c}$	6×10^{-5}	m
$B_{\nu 0}^{\tau}$	6×10^{-5}	m
α_1	20	–

where a maximum load of 47 kN is observed with a displacement of approximately 0.8 mm, and a maximum displacement of 1.75 mm, which are graphically compared in Fig. 13.5. As Lourenço indicated in his doctoral thesis [4], the normal and tangential rigidities are directly related to Young's module and the shear modulus, respectively. Where it is also known that the shear modulus is smaller than the Young module in masonry, which is also reflected in the values of the normal and tangential stiffnesses indicated in Table 13.1. On the other hand, it is valid to mention the presence of friction, which is characteristic in masonry, due to the α_1 parameter.

In addition, by analyzing Fig. 13.6 of the evolution of damage in masonry, the behavior of the Force-Displacement curve can be explained. As iterations progress, damage in the normal (compression) and tangential direction increases until the maximum force is reached. Then, damage in the normal direction remains constant, while tangential damage continues to increase until it reaches its maximum, leading to softening.
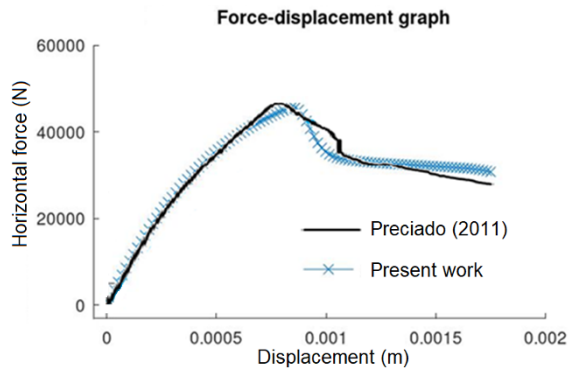
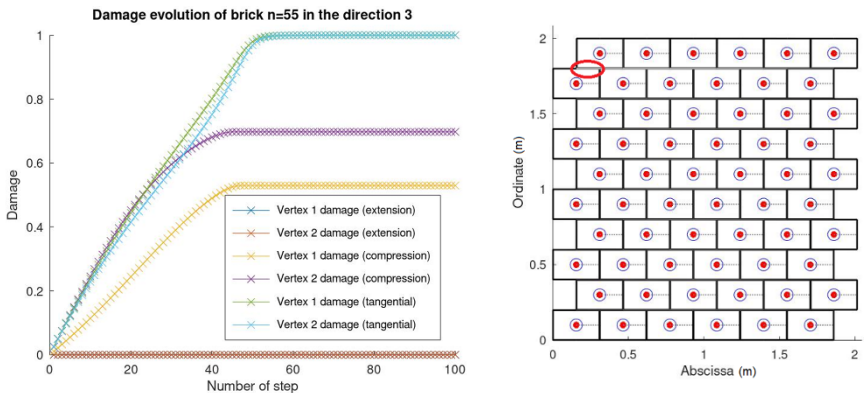**Fig. 13.5** Comparison of force-displacement graphs.

Fig. 13.6: Evolution of damage with respect to iterations in a specific part of the masonry.

13.3.2 Influence of Mortar Thickness on Masonry Performance

In order to evaluate the influence of the mortar thickness on the masonry, three scenarios will be evaluated, where each will have different mortar thicknesses, but the rest of parameters will remain constant (Fig. 13.7). These thicknesses correspond to 10, 20 and 30 mm (Table 13.2). In addition, the elastic rigidities and the parameters constituting the damage correspond to the values of Table 13.1. For the three cases, a standard brick geometry corresponding to 215 x 65 mm in width and height respectively shall be used, where a horizontal monotone force shall be applied to the upper left corner.

When evaluating these scenarios, Force-Displacement curves were obtained for each case. As can be seen in Figure 13.8, as the mortar thickness is reduced, the maximum horizontal force that the masonry supports is reduced. It is common to observe in some studies as in Caldeira et al. [47], where it is reported that a high mortar thickness may be susceptible to cause a weakening in the structural behavior
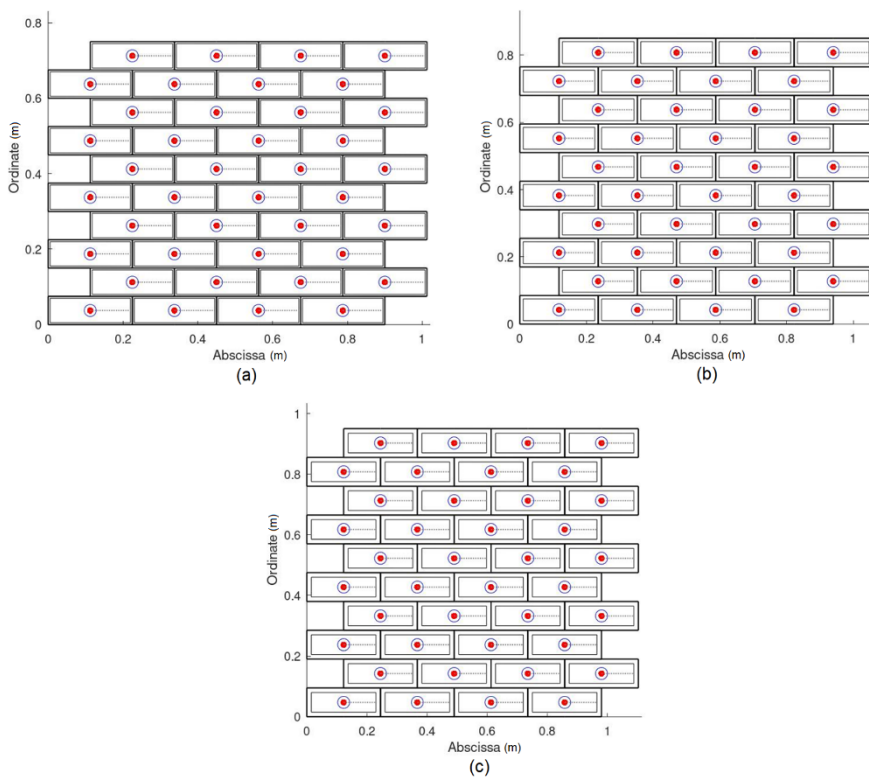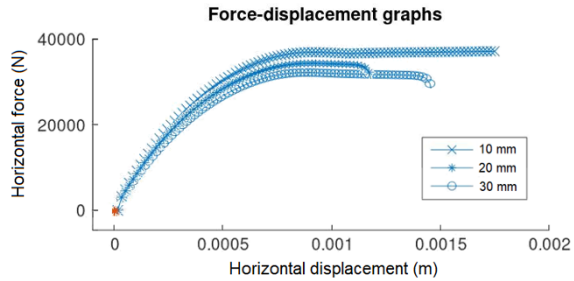

Fig. 13.7: Masonry with different mortar thicknesses. (a) 10 mm (b) 20 mm (c) 30 mm.

Table 13.2: Geometric parameters corresponding to the augmented bricks.

Thickness (l_m)	Width (l_x)	Height (l_y)
10 mm	0.225 m	0.075 m
20 mm	0.235 m	0.085 m
30 mm	0.245 m	0.095 m

Fig. 13.8 Force-Displacement graphics according to mortar thickness.


of masonry in general. In the model, this could be reflected in the decrease of the maximum force in the Force-Displacement curves.

13.3.3 Bending and Shear Sliding

With the aim of studying the bending and shear sliding phenomena in masonry walls reported in several studies as in [48]-[50], a scenario will be evaluated where the characteristic length of damage *B* will be modified. In the same way, the reference values of Table 13.1 will be taken for a first case and, for the second case, the value of B that will be the same in the normal and tangential direction, will be reduced. The graphical result is shown in Fig. 13.9, where, in the case of the reference value B, the wall tends to produce a bending, whereas, in the case of the reduced value B, the wall tends to slide by shear. It is then said that, the wall will fail by shear as long as the value of the characteristic length of the damage B is reduced, which has a direct relation with the properties of the mortar. Figure 13.10 shows in greater detail the movement of the bricks for each type of wall failure evaluated.

This is corroborated in some studies [51], where it is mentioned that this phenomenon of sliding by shear is produced when poor or weak mortar mixtures are present and there are low axial forces on the top of the wall.

(a)

(b)
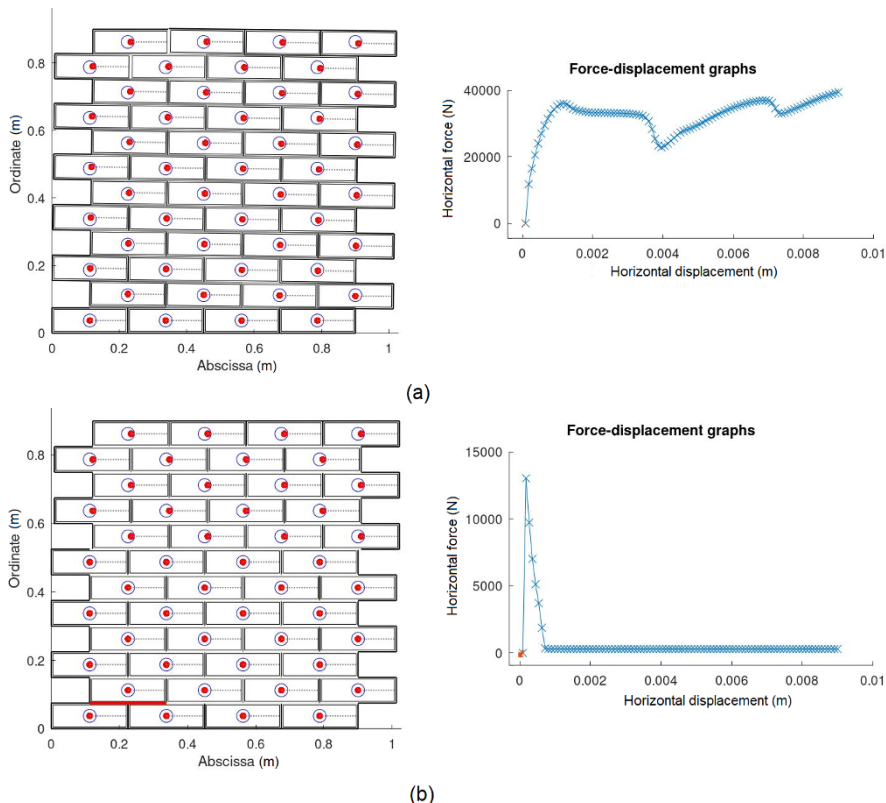
Fig. 13.9: Masonry and its respective Force-Displacement curves. (a) Bending $B = 6 \times 10^{-5}$ m (b) Shear sliding $B = 6 \times 10^{-6}$ m.

Fig. 13.10 Row number five (from the top): (a) bending, (b) shear sliding.

(a)

(b)
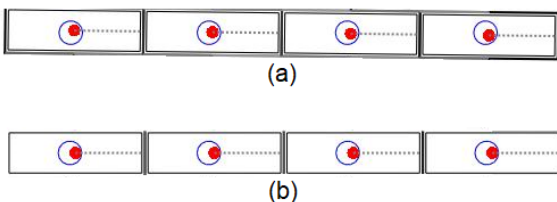
13.3.4 Rocking

The rocking phenomenon has also been reported in numerous studies evaluating in-plane failures of simple masonry walls [48]-[50]. For the present work, it will be sought to simulate the same behavior, depending on the parameters used previously and the displacements imposed on the wall, which are calculated as forces.

The parameters correspond to those of Table 13.1 and Table 13.2 for a masonry of 10 mm thick mortar. The imposed displacements (u_x, u_y) correspond to (0.02 m,

0.02 m). In addition, the damage characteristic length values in Table 13.3 were used. The results in Fig. 13.11 show that due to the vertical and horizontal displacements imposed, the masonry tends to balance with respect to the lower right, where in addition a failure in the base is observed. It is important to note that this also occurs due to the embedding of the base with respect to the wall.

## 13.4 Conclusions and Future Challenges

The study that has been developed is an extension of what was done by Tran et al. [33], who worked on a structure of nine bricks, while the present work has been developed on structures with a greater number of bricks. Thus, it has been possible to monitor each of the augmented bricks, allowing to detect various types of shear, bending and rocking failures.

The results obtained show an acceptable approximation by the proposal of Tran et al. [33] of previous investigations made in this regard, as is the case of Preciado [46]. From this, it has been possible to detect some characteristic properties in masonry as the case of friction and a tangential stiffness less than the normal stiffness.

The thickness of the mortar layer influences the structural behavior of a wall, although this behavior will depend on whether the wall is subjected to compression or tension. In the case of a wall subjected to compression, as is the case with the load-bearing walls, it has been observed that, the smaller the thickness of the mortar

Table 13.3: Characteristic lengths of damage.

Parameter	Value	Unit
$B_\nu^{\eta,t}$	3×10^{-5}	m
$B_\nu^{\eta,c}$	3×10^{-5}	m
$B_{\nu 0}^{\tau}$	3×10^{-5}	m
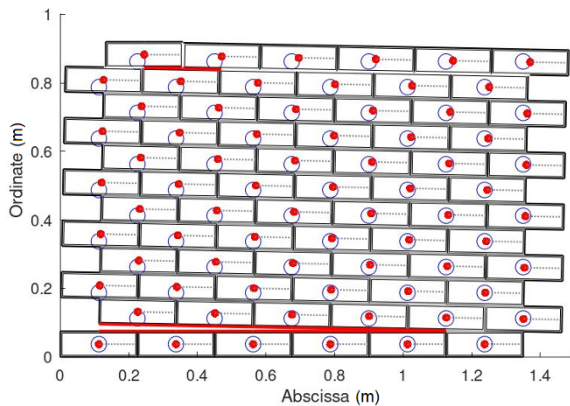
Fig. 13.11 Rocking in masonry wall.

layer, the lower the damage. This has been observed in the present work, for the case of the evaluation of the influence of the mortar thickness on the walls.

While it is true that anti-seismic structures require a certain ductility that allows a controlled deformation, and thereby reduce seismic energy, a sharp reduction in the rigidity of the mortar could cause its resistance to shearing to decrease, causing a potential displacement of one row or set of rows from others, as evidenced by the results of shear sliding.

The model of Tran et al. [33] assumes that a brick has an infinite rigidity, so that the only element that has the possibility of failure is the mortar. This hypothesis should be reviewed and the rigidity of a brick and its possible fracture incorporated into the model. Therefore, the proposed model does not explain the diagonal failure that a wall may present, due to a failure by shearing of the bricks. In this respect, it would be desirable for the model consider the failure lines of the bricks and the evolution of these during the iterations.

References

[1] Derakhshan H, Griffith MC. Ingha, JM (2016) Out-of-plane seismic response of vertically spanning urm walls connected to flexible diaphragms, Earthquake Engineering & Structural Dynamics **45**(4):563-580.

[2] Quinteros RD (2014) Modelización del comportamiento de estructuras de mampostería mediante la teoría de homogeneización, Ph.D. thesis, Tesis doctoral, Facultad de Ingeniería, Universidad Nacional de Salta.

[3] Polyakov S (1960) On the interaction between masonry filler walls and enclosing frame when loaded in the plane of the wall, Translations in Earthquake Engineering **2**(3):36-42.

[4] Lourenço P (1996) Computational strategies for masonry structures [ph. d. thesis], Civil Engineering and Geosciences. Eindhoven, Netherland, Delft University.

[5] Xu C, Xiangli C, Bin L (2012) Modeling of influence of heterogeneity on mechanical performance of unreinforced masonry shear walls, Construction and Building Materials **26**(1):90-95.

[6] Bilotta A, Turco E (2017) Elastoplastic analysis of pressure-sensitive materials by an effective three-dimensional mixed finite element, ZAMM-Journal of Applied Mathematics and Mechanics/Zeitschrift für Angewandte Mathematik und Mechanik **97**(4):382-396.

[7] Tedesco F, Bilotta A, Turco E (2017) Multiscale 3d mixed fem analysis of historical masonry constructions, European Journal of Environmental and Civil Engineering **21**(7-8):772-797.

[8] Berdichevsky VL (2009) Variational principles. In: Variational Principles of Continuum Mechanics, pp 3-44. Springer.

[9] dell'Isola F, Eugster SR, Spagnuolo M, Barchiesi E (2021) Evaluation of Scientific Sources in Mechanics: Heiberg's Prolegomena to the Works of Archimedes

and Hellinger's Encyclopedia Article on Continuum Mechanics, Advanced Structured Materials, vol. 152, Springer Nature.

[10] dell'Isola F, Della Corte A (2020) History of the Principle of Virtual Work. In: Encyclopedia of Continuum Mechanics, pp 1190–1197, Springer.

[11] dell'Isola F, Placidi L (2011) Variational principles are a powerful tool also for formulating field theories, In: Variational models and methods in solid and fluid mechanics, pp 1–15. Springer.

[12] dell'Isola F, Andreaus U, Placidi L (2015) At the origins and in the vanguard of peridynamics, non-local and higher-gradient continuum mechanics: an underestimated and still topical contribution of Gabrio Piola, Mathematics and Mechanics of Solids **20**(8):887-928.

[13] dell'Isola F, Corte AD, Giorgio I (2017) Higher-gradient continua: The legacy of piola, mindlin, sedov and toupin and some future research perspectives, Mathematics and Mechanics of Solids **22**(4):852-872.

[14] Barchiesi E, Hamila N: Maximum mechano-damage power release-based phase-field modeling of mass diffusion in damaging deformable solids, Zeitschrift für angewandte Mathematik und Physik **73**(1):1-21.

[15] Maugin GA (2013) The principle of virtual power: from eliminating metaphysical forces to providing an efficient modelling tool, Continuum Mechanics and Thermodynamics **25**(2):127-146.

[16] Tran CA, Gołaszewski M, Barchiesi E (2020) Symmetric-in-plane compression of polyamide pantographic fabrics–modelling, experiments and numerical exploration, Symmetry **2020**(12):693.

[17] Abali BE, Müller WH, dell'Isola F (2017) Theory and computation of higher gradient elasticity theories based on action principles, Archive of Applied Mechanics **87**(9):1495-1510.

[18] Auffray N, dell'Isola F, Eremeyev VA, Madeo A, Rosi G (2015) Analytical continuum mechanics à la Hamilton–Piola least action principle for second gradient continua and capillary fluids, Mathematics and Mechanics of Solids **20**(4):375-417.

[19] Giorgio I (2021) Lattice shells composed of two families of curved Kirchhoff rods: an archetypal example, topology optimization of a cycloidal metamaterial, Continuum Mechanics and Thermodynamics **33**(4):1063-1082.

[20] dell'Isola F, Seppecher P, Placidi L, Barchiesi E, Misra A (2020) Least action and virtual work principles for the formulation of generalized continuum models, Discrete and Continuum Models for Complex Metamaterials, pp 327-394 (2020)

[21] Germain P (1973) The method of virtual power in continuum mechanics. Part 2: Microstructure, SIAM Journal on Applied Mathematics **25**(3):556-575.

[22] Germain P (2020) The method of virtual power in the mechanics of continuous media, I: Second-gradient theory, Mathematics and Mechanics of Complex Systems **8**(2):153-190.

[23] Maugin G (1980) The method of virtual power in continuum mechanics: application to coupled fields, Acta Mechanica **35**(1):1-70.

[24] Placidi L, Barchiesi E, dell'Isola F, Maksimov V, Misra A, Rezaei N, Scrofani A, Timofeev D (2020) On a hemi-variational formulation for a 2D elasto-plastic-

damage strain gradient solid with granular microstructure, Mathematics in Engineering **5**(1):1-24.

[25] Giorgio I (2020) A discrete formulation of Kirchhoff rods in large-motion dynamics, Mathematics and Mechanics of Solids **25**(5):1081-1100.

[26] Turco E, Barchiesi E, Giorgio I, dell'Isola F (2020) A Lagrangian Hencky-type non-linear model suitable for metamaterials design of shearable and extensible slender deformable bodies alternative to Timoshenko theory, International Journal of Non-Linear Mechanics **123**:103481.

[27] Alibert JJ, Seppecher P, dell'Isola F (2003) Truss modular beams with deformation energy depending on higher displacement gradients, Mathematics and Mechanics of Solids **8**(1):51-73.

[28] Baroudi D, Giorgio I, Battista A, Turco E, Igumnov LA (2019) Nonlinear dynamics of uniformly loaded elastica: Experimental and numerical evidence of motion around curled stable equilibrium configurations, ZAMM-Journal of Applied Mathematics and Mechanics/Zeitschrift für Angewandte Mathematik und Mechanik **99**:e201800121

[29] Turco E, Barchiesi E (2019) Equilibrium paths of Hencky pantographic beams in a three-point bending problem, Mathematics and Mechanics of Complex Systems **7**(4):287–310.

[30] Misra A, Placidi L, Turco E (2020) Variational methods for discrete models of granular materials, Encyclopedia of Continuum Mechanics, pp 2621-2634.

[31] Turco E, Misra A, Pawlikowski M, dell'Isola F, Hild F (2018) Enhanced Piola–Hencky discrete models for pantographic sheets with pivots without deformation energy: numerics and experiments, International Journal of Solids and Structures **147**:94-109.

[32] dell'Isola F, Giorgio I, Pawlikowski M, Rizzi NL (2016) Large deformations of planar extensible beams and pantographic lattices: heuristic homogenization, experimental and numerical examples of equilibrium, Proceedings of the Royal Society A: Mathematical, Physical and Engineering Sciences **472**(2185):20150790.

[33] Tran CA, Barchiesi E, Placidi L, León Trujillo FJ (2021) A block-based variational elasto-damage model for masonry analysis inspired from granular micromechanics: Preliminary study, Mechanics Research Communications **118**:103802.

[34] Gagliardo R, Portioli F, Cascini L, Landolfo R, Lourenço P (2021) A rigid block model with no-tension elastic contacts for displacement-based assessment of historic masonry structures subjected to settlements, Engineering Structures **229**:111609.

[35] Pepe M, Sangirardi M, Reccia E, Pingaro M, Trovalusci P, De Felice G (2020) Discrete and continuous approaches for the failure analysis of masonry structures subjected to settlements, Frontiers in Built Environment **6**:43.

[36] Portioli FP, Godio M, Calderini C, Lourenço PB (2021) A variational rigid-block modeling approach to nonlinear elastic and kinematic analysis of failure mechanisms in historic masonry structures subjected to lateral loads, Earthquake Engineering & Structural Dynamics **50**(12):3332-3354.

[37] Placidi L, Barchiesi E, Misra A, Timofeev D (2021) Micromechanics-based elasto-plastic-damage energy formulation for strain gradient solids with granular microstructure, Continuum Mechanics and Thermodynamics **33**:2213–2241.

[38] Placidi L, Misra A, Barchiesi E (2019) Simulation results for damage with evolving microstructure and growing strain gradient moduli, Continuum Mechanics and Thermodynamics **31**(4):1143-1163.

[39] Misra A, Singh V: Nonlinear granular micromechanics model for multi-axial rate-dependent behavior, International Journal of Solids and Structures **51**(13):2272-2282.

[40] Barchiesi E, Misra A, Placidi L, Turco E (2021) Granular micromechanics-based identification of isotropic strain gradient parameters for elastic geometrically nonlinear deformations, ZAMM-Journal of Applied Mathematics and Mechanics/Zeitschrift für Angewandte Mathematik und Mechanik **101**:e202100059.

[41] Maksimov V. Barchiesi E, Misra A, Placidi L, Timofeev D (2021) Two-dimensional analysis of size effects in strain-gradient granular solids with damage-induced anisotropy evolution, Journal of Engineering Mechanics **147**(11):04021098-1.

[42] Nejadsadeghi N, Misra A (2020) Extended granular micromechanics approach: a micromorphic theory of degree n, Mathematics and Mechanics of Solids **25**(2):407-429.

[43] Giorgio I, dell'Isola F, Misra A (2020) Chirality in 2D Cosserat media related to stretch-micro-rotation coupling with links to granular micromechanics, International Journal of Solids and Structures **202**:28-38.

[44] Misra A, Poorsolhjouy P (2017) Grain-and macro-scale kinematics for granular micromechanics based small deformation micromorphic continuum model, Mechanics Research Communications **81**:1-6.

[45] Timofeev D, Barchiesi E, Misra A, Placidi L (2021) Hemivariational continuum approach for granular solids with damage-induced anisotropy evolution. Mathematics and Mechanics of Solids **26**(5):738-770.

[46] Preciado Quiroz A (2011) Seismic vulnerability reduction of historical masonry towers by external prestressing devices, Ph.D. thesis, Dissertation, Braunschweig, Technische Universität Braunschweig.

[47] Caldeira FE, Nalon GH, de Oliveira DS, Pedroti LG, Ribeiro JCL, Ferreira FA, de Carvalho JMF (2020) Influence of joint thickness and strength of mortars on the compressive behavior of prisms made of normal and high-strength concrete blocks, Construction and Building Materials **234**:117419.

[48] D'Altri AM, Sarhosis V, Milani G, Rots J, Cattari S, Lagomarsino S, Sacco E, Tralli A, Castellazzi G, de Miranda S (2020) Modeling strategies for the computational analysis of unreinforced masonry structures: review and classification, Archives of Computational Methods in Engineering **27**:1153–1185

[49] Dong F, Wang H., Jiang F, Xing Q, Yu J: In-plane shear behavior of masonry panels strengthened with ultra-high ductile concrete (HHDC), Engineering Structures **252**:113609.

[50] Mezrea PE, Ispir M, Balci IA, Bal IE, Ilki A (2021) Diagonal tensile tests on historical brick masonry wallets strengthened with fabric reinforced cementitious mortar, Structures **33**:935-946.

[51] Celano T, Argiento LU, Ceroni F, Casapulla C (2021) Literature review of the in-plane behavior of masonry walls: Theoretical vs. experimental results, Materials **14**(11):3063.